Nonthermal broadening in the conductance of double quantum dot structures

L. Oroszlány,[1] A. Kormányos,[1] J. Koltai,[2] J. Cserti,[3] and C. J. Lambert[1]
[1]*Department of Physics, Lancaster University, Lancaster LA1 4YB, United Kingdom*
[2]*Department of Biological Physics, Eötvös University, Pázmány Péter Sétány 1/A, H-1117 Budapest, Hungary*
[3]*Department of Physics of Complex Systems, Eötvös University, Pázmány Péter Sétány 1/A, H-1117 Budapest, Hungary*
(Received 26 January 2007; revised manuscript received 25 April 2007; published 17 July 2007)

We study the transport properties of a double quantum dot (DQD) molecule at zero and at finite temperature. The properties of the zero-temperature conductance depend on whether the level attraction between the symmetric and antisymmetric states of the DQD, produced by the coupling to the leads, exceeds or not the interdot tunneling. For finite temperature, we find a remarkable nonthermal broadening effect of the conductance resonance when the energy levels of the individual dots are detuned.

DOI: 10.1103/PhysRevB.76.045318 PACS number(s): 73.21.La, 73.23.−b, 73.63.Kv

I. INTRODUCTION

Double quantum dot (DQD) systems exhibit a wide range of interesting and fundamental physical phenomena, such as Coulomb blockade oscillations of conductance,[1–10,16] the formation of "double quantum dot molecule,"[9–25] or the Kondo effect.[26–29] Experimentally, DQDs have been formed in semiconductor heterostructures,[4,5,12–19] in single wall carbon nanotubes,[20–23] and in InAs nanowires.[24,25] In recent years, interest in DQDs has also been driven by the quest for a solid-state based qubit, the elementary building block of a quantum computer. In the presence of an interdot coupling t_c, coherent electron states can extend over the whole DQD system, resembling therefore the formation of chemical bonds in molecules. This interdot coupling t_c controls the exchange interaction of electron spins, assumed to be localized in each of the dots, and hence eventually the operation of a corresponding solid-state qubit system[30] as well.

Another interesting phenomenon, seen in experiments[16] performed in the Coulomb blockade regime at high source-drain voltages, is that the levels of one of the quantum dots (QDs) can act as a low-temperature filter for the other QD. This means that on detuning the energies of the levels participating in the resonant tunneling process, the width of the resonance peak in conductance is independent of the temperature.

Surprisingly, a complete analytical description of nonthermal broadening is not currently available, despite the fact that this effect is alluded to in the early work of Ref. 1 and has been demonstrated numerically in Ref. 11 for coherently coupled quantum dots at large source-drain voltages $e|V| \gg t_c$. A complete analytical theory of coherently coupled dots is desirable, since in all the above theories, the shape of the resonant peak is found to be Lorentzian. Experimentally, non-Lorentzian line shapes are found, but these are attributed to inelastic scattering. It is therefore of interest to ask under what circumstances non-Lorentzian peaks are found in the absence of inelastic scattering.

In this paper, we consider a DQD system with coherent interdot coupling as well as with coherent couplings between the dots and leads. We assume that the charging energies of the dots are negligible or can be treated as constant shifts[3] and therefore the system can be described by an effective single-particle model. (For studies of the electronic correlations in DQDs, see Refs. 36–40.) We note that experimental results on DQD molecules are often explained with such simple effective single-particle models,[15,18–20] which usually assume that couplings of the dots to the leads can be neglected. We first show how the finite interdot and dot-lead couplings affect the line shape of the zero-bias conductance resonance. Our results are nonperturbative and take into account all orders of interdot and dot-lead tunnel processes. We also consider the finite-temperature conductance and present results for the temperature dependence of the peak height of the conductance resonance as well as its broadening. We show that in our model, the nonthermal broadening effect in resonant transport can be observed even in the zero-bias limit, if the dot-lead coupling strength exceeds the interdot coupling t_c.

The paper is organized as follows. In Sec. II, we introduce a very general description of coupled dots and derive the zero-temperature transmission formula. In Sec. III, we discuss the properties of the zero-temperature and zero-bias conductance as functions of the energy levels of the two dots and of the various couplings in the systems. In Sec. IV, we derive a finite-temperature conductance formula for the DQD system and discuss temperature-dependent transport properties of the system.

II. MODEL

We consider two quantum dots coupled to left and right leads with tunnel coupling Γ_L and Γ_R, respectively, as shown in Fig. 1(a). The interdot tunneling coupling is denoted by t_c and it is assumed that only one energy level in each dot is relevant. The intradot as well as the interdot Coulomb interactions are neglected.

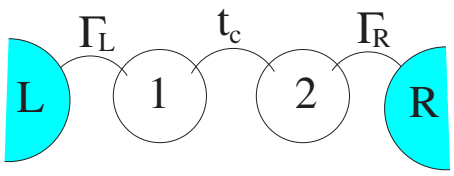

FIG. 1. (Color online) Double quantum dot coupled to left (L) and right (R) leads with interdot coupling t_c.

As shown in Appendix A, the electron transmission coefficient $T_{dd}(E)$ of the double dot system can be written as

$$T_{dd}(E) = \frac{4\Gamma_L\Gamma_R t_c^2}{|E-E_+|^2|E-E_-|^2}. \quad (1)$$

Here, $E_\pm$ are the poles of the transmission:

$$E_\pm = \bar{\varepsilon} + i\bar{\Gamma} \pm \sqrt{(\Delta\varepsilon + i\Delta\Gamma)^2 + t_c^2}, \quad (2)$$

where $\bar{\varepsilon}=(\tilde{\varepsilon}_1+\tilde{\varepsilon}_2)/2$, $\bar{\Gamma}=(\Gamma_L+\Gamma_R)/2$ is the total coupling strength to the leads, while $\Delta\varepsilon=(\tilde{\varepsilon}_1-\tilde{\varepsilon}_2)/2$, $\Delta\Gamma=(\Gamma_L-\Gamma_R)/2$ are the asymmetries of the dot energies and the couplings to the leads, respectively.

Having obtained the transmission function $T_{dd}(E)$, the linear conductance at finite temperature is given by

$$\mathcal{G}_T = \frac{2e^2}{h}\int_0^\infty T_{dd}(E)\left[-\frac{\partial f_0(E)}{\partial E}\right]dE, \quad (3)$$

where $f_0(E)=\{1+\exp[(E-\mu)/k_BT]\}^{-1}$ is the equilibrium Fermi distribution, μ being the chemical potential of the leads. For $k_BT \ll E_F$, we can take $\mu \approx E_F$ and extend the lower bound of the integration to $-\infty$ in Eq. (3). The resulting integral can then be calculated by contour integration. The zero-temperature transmission $T_{dd}(E)$ has only simple poles if $|\Delta\Gamma| \neq t_c$, $\Delta\varepsilon \neq 0$ and the finite-temperature conductance reads

$$\mathcal{G}_T = \frac{2e^2}{h}\frac{\Gamma_L\Gamma_R t_c^2}{\pi(k_BT)^4}\left\{\frac{1}{(\omega_+-\omega_-)}\left[\frac{1}{\Im\omega_+(\omega_+-\omega_-^*)}\psi^{(1)}\left(\frac{1}{2}-\frac{i\omega_+}{2\pi}\right)\right.\right.$$
$$\left.\left.+\frac{1}{\Im\omega_-(\omega_+^*-\omega_-)}\psi^{(1)}\left(\frac{1}{2}-\frac{i\omega_-}{2\pi}\right)\right]+\text{c.c.}\right\}, \quad (4)$$

where $\psi^{(1)}(z)$ is the first polygamma function,[31] $\omega_\pm=(E_\pm-E_F)/k_BT$ [here, $E_\pm$ are the poles of $T_{dd}(E)$ in the upper half complex plain, given by Eq. (2)], $\Im$ denotes the imaginary part, and * stands for complex conjugation. In the case of $\Delta\varepsilon=0$ and $|\Delta\Gamma|=t_c$, the transmission $T_{dd}(E)$ has second order poles and therefore $\mathcal{G}_T$ is given by

$$\mathcal{G}_T = \frac{e^2}{h}\frac{\Gamma_L\Gamma_R t_c^2}{\pi k_BT}\frac{1}{(\Im\omega)^3}\left[\psi^{(1)}\left(\frac{1}{2}-\frac{i\omega}{2\pi}\right)\right.$$
$$\left.-\frac{\Im\omega}{2\pi}\psi^{(2)}\left(\frac{1}{2}-\frac{i\omega}{2\pi}\right)+\text{c.c.}\right]. \quad (5)$$

Here, $\omega=(\bar{\varepsilon}-E_F+i\bar{\Gamma})/k_BT$ and $\psi^{(2)}(z)$ is the second polygamma function.[31]

In what follows, we briefly discuss the properties of the zero-temperature conductance with emphasis on the effect of couplings Γ_L, Γ_R, and t_c. The understanding of the zero-temperature case then helps us to interpret the finite-temperature behavior of the conductance in Sec. IV.

III. ZERO-TEMPERATURE LINEAR CONDUCTANCE

From Eq. (3), the linear conductance $\mathcal{G}_0$ at zero temperature is given by the Landauer formula[32]

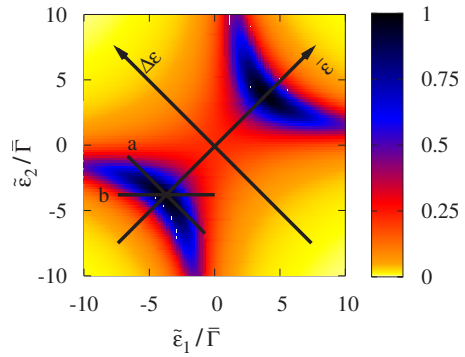

FIG. 2. (Color online) Zero-temperature conductance at $E=E_F$ as a function of $\tilde{\varepsilon}_1$, $\tilde{\varepsilon}_2$ for $t_c \gg \Lambda$. For details, see text.

$$\mathcal{G}_0 = \frac{2e^2}{h}T_{dd}(E_F). \quad (6)$$

Using Eqs. (1) and (2), one can obtain an explicit expression for $\mathcal{G}_0$ as a function of E_F and the characteristic energies of the DQD system: $\tilde{\varepsilon}_1$, $\tilde{\varepsilon}_2$, $\bar{\Gamma}$, $\Delta\Gamma$, and t_c. For $\Delta\Gamma=0$, this expression agrees with the result obtained in Ref. 33 for serially connected dots but otherwise also describes the case when $\Delta\Gamma \neq 0$. In an experiment, E_F would be kept fixed and the energy levels of the dots as well as the tunnelings to the leads would be changed by side and top gates. Therefore, in what follows, without loss of generality, we can set $E_F=0$.

Our aim is to understand the properties of the conductance in the $(\tilde{\varepsilon}_1,\tilde{\varepsilon}_2)$ plane [or equivalently, in $(\bar{\varepsilon},\Delta\varepsilon)$ plane, where $\bar{\varepsilon}$ and $\Delta\varepsilon$ are defined after Eq. (2)]. It follows from Eq. (1) that depending on the ratio t_c^2/Λ, where $\Lambda=\sqrt{(\Gamma_L^2+\Gamma_R^2)/2}$, the conductance has either one or two maxima in the $(\tilde{\varepsilon}_1,\tilde{\varepsilon}_2)$ plane. As shown in Fig. 2, for $t_c \gg \Lambda$, the conductance is enhanced in two boomerang-shaped regions, while for $t_c \ll \Lambda$, there is one maximum in the conductance at $\tilde{\varepsilon}_1=\tilde{\varepsilon}_2=E_F$ (see Fig. 3).

To see the dependence of the conductance on the energy levels of the dots and on the various couplings in the system, we now consider certain directions in the $(\tilde{\varepsilon}_1,\tilde{\varepsilon}_2)$ plane and study the cross sections of the conductance along these directions. Let us first assume that the levels $\tilde{\varepsilon}_1$, $\tilde{\varepsilon}_2$ of the two

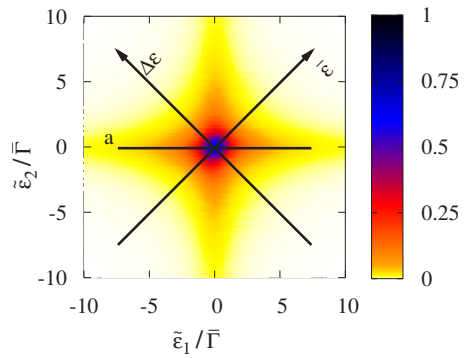

FIG. 3. (Color online) Zero-temperature conductance at $E=E_F$ as a function of $\tilde{\varepsilon}_1$, $\tilde{\varepsilon}_2$ for $t_c \ll \Lambda$. For details, see text.

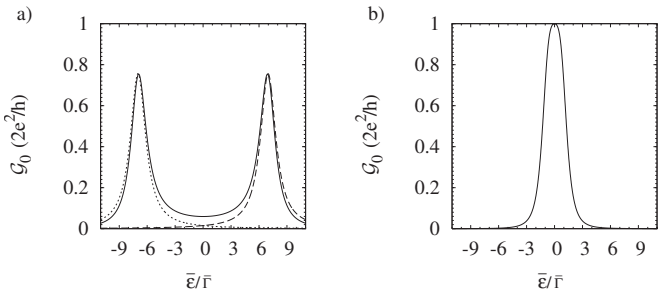

FIG. 4. (a) Conductance for $t_c \gg \Lambda$ along the $\bar{\varepsilon}$ axis using Eq. (1) (solid line). The approximation given by Eq. (8) is shown with dashed lines. We used $t_c/\bar{\Gamma}=7$ and $\Delta\Gamma/\bar{\Gamma}=0.5$. (b) The transmission for $t_c=\sqrt{\Gamma_L\Gamma_R}<\Lambda$ given by Eq. (9). The parameters are $t_c/\bar{\Gamma}=0.954$ and $\Delta\Gamma/\bar{\Gamma}=0.3$. For details, see text.

dots are kept aligned, i.e., $\Delta\varepsilon=0$ and we study $\mathcal{G}_0$ along the $\bar{\varepsilon}$ axis.

If $t_c>\Lambda$, upon varying $\bar{\varepsilon}$, two resonances occur in the conductance [see Figs. 2 and 4(a)] at energies

$$\bar{\varepsilon}_\pm = \pm\sqrt{t_c^2-\Lambda^2}, \tag{7}$$

corresponding to symmetric (−) and antisymmetric (+) molecular states. Note that in an isolated double dot molecule where $\Gamma_L=\Gamma_R=0$, the energies of the symmetric (antisymmetric) states are $\bar{\varepsilon}_\pm^0=\pm t_c$. Thus, Eq. (7) shows that connection to the leads produces level attraction. Since $\Lambda=\sqrt{\bar{\Gamma}^2+\Delta\Gamma^2}$, the magnitude of the level attraction depends both on the total coupling strength $\bar{\Gamma}$ and on the asymmetry $\Delta\Gamma$ of the couplings. Similar level attraction has been reported in Ref. 33 for QDs attached in parallel to the leads and in Ref. 34 for an Aharonov-Bohm ring with a quantum dot in each of its arms. It can also be shown that $\mathcal{G}_0$ reaches the quantum limit $2e^2/h$ at energies given by Eq. (7) only if $\Delta\Gamma=0$, i.e., for symmetric couplings to the leads. For $t_c \gg \Lambda$, when the two resonances are well separated, the line shape around $\bar{\varepsilon}=\pm\sqrt{t_c^2-\Lambda^2}$ is approximately a Lorentzian of linewidth $\bar{\Gamma}$:

$$\mathcal{G}_0(\bar{\varepsilon}) \approx \frac{2e^2}{h}\frac{t_c^2}{[t_c^2-(\bar{\Gamma}^2/4+\Delta\Gamma^2)]}\frac{\Gamma_L\Gamma_R}{[(\bar{\varepsilon}\pm\sqrt{t_c^2-\Delta\Gamma^2})^2+\bar{\Gamma}^2]}. \tag{8}$$

Regarding the enhancement of the conductance in a boomerang-shaped areas in the $(\tilde{\varepsilon}_1,\tilde{\varepsilon}_2)$ plane (see Fig. 2), it is easy to prove that if $\Delta\Gamma=0$, for a given value of $\Delta\varepsilon$, the transmission T_{dd} has maximum at $\bar{\varepsilon}=\pm\sqrt{\Delta\varepsilon^2+t_c^2-\Gamma^2}$. This is the equation of a hyperbola in the $(\bar{\varepsilon},\Delta\varepsilon)$ plane and also helps to understand the observed structure of the conductance when $t_c \gg |\Delta\Gamma| \neq 0$, which is the case in Fig. 2.

The separation between the two resonances decreases as Λ is increased while keeping t_c fixed. Finally, the two resonances merge when $\Lambda=t_c$, meaning that due to the coupling to the leads, the energies of the symmetric and antisymmetric states become degenerate at this value of Λ. For $\Lambda>t_c$, the conductance then has only one resonance at energy $\bar{\varepsilon}=E_F$ [see Figs. 3 and 4(b)] and, from Eqs. (1) and (2), has the form

$$\mathcal{G}_0(\bar{\varepsilon}) = \frac{2e^2}{h}\frac{4\Gamma_L\Gamma_R\tilde{t}_c^2}{[(\bar{\varepsilon}+\tilde{t}_c)^2+\Gamma_+^2][(\bar{\varepsilon}-\tilde{t}_c)^2+\Gamma_-^2]}. \tag{9}$$

Here, $\tilde{t}_c=\sqrt{t_c^2-\Delta\Gamma^2}$, $\Gamma_\pm=\bar{\Gamma}$ if $|\Delta\Gamma|\leqslant t_c\leqslant\bar{\Gamma}$ and one can show that the conductance on resonance $\mathcal{G}_0(\bar{\varepsilon}=E_F)$ is smaller than $2e^2/h$ except for the special case $t_c=\sqrt{\Gamma_L\Gamma_R}$ (Ref. 41) [see Fig. 4(b)]. On the other hand, if $t_c<|\Delta\Gamma|<\bar{\Gamma}$, we have $\tilde{t}_c=0$ and $\Gamma_\pm=\bar{\Gamma}\pm\sqrt{\Delta\Gamma^2-t_c^2}$ in Eq. (9), and we find that $\mathcal{G}_0(\bar{\varepsilon})<2e^2/h$ for all $\bar{\varepsilon}$. Thus, for $t_c<\Lambda$, the line shape of the resonance can again be approximated by a Lorentzian around $\bar{\varepsilon}=E_F$ but for larger $|\bar{\varepsilon}|$, it decreases as $\sim 1/\bar{\varepsilon}^4$.

Further understanding of the properties of the conductance can be gained by considering $\Delta\varepsilon\neq 0$, i.e., finite detuning between the levels of the (isolated) dots. In principle, one could follow any path in the $(\tilde{\varepsilon}_1,\tilde{\varepsilon}_2)$ plane to study the effect of finite $\Delta\varepsilon$, but let us consider two simple yet important cases. Let us first assume that $\bar{\varepsilon}$ is kept fixed at the value where the conductance is largest and we vary only $\Delta\varepsilon$, i.e., we study the conductance parallel to the $\Delta\varepsilon$ axis. Analytical progress can be made most easily for $\Delta\Gamma=0$, i.e., $\Gamma_L=\Gamma_R=\Gamma$.

When $t_c>\Lambda=\Gamma$ and $\bar{\varepsilon}=\bar{\varepsilon}_\pm$, i.e., $\bar{\varepsilon}$ equals the energy of the symmetric (antisymmetric) state, the conductance as a function of $\Delta\varepsilon$ reads

$$\mathcal{G}_0(\Delta\varepsilon) = \frac{2e^2}{h}\frac{4\Gamma^2t_c^2}{\Delta\varepsilon^2(\Delta\varepsilon^2+4\Gamma^2)+4\Gamma^2t_c^2}. \tag{10}$$

[This corresponds to taking the cross section of $T_{dd}(E)$ along the line denoted by "a" in Fig. 2.] We see that the line shape is basically a Lorentzian for $\Delta\varepsilon\ll\Gamma$ but falls more rapidly for $\Delta\varepsilon\gtrsim\Gamma$. The full width at half maximum (FWHM) is $\Delta\varepsilon_W=2\sqrt{2\Gamma(\sqrt{\Gamma^2+t_c^2}-\Gamma)}$, which simplifies to $\Delta\varepsilon_W\approx 2\sqrt{2\Gamma(t_c-\Gamma)}$ for $t_c\gg\Gamma$.

Another obvious way to study the effect of finite $\Delta\varepsilon$ is to fix one of the energies (e.g., $\tilde{\varepsilon}_2$) and vary only $\tilde{\varepsilon}_1$. In contrast with the previous example, this means that both $\bar{\varepsilon}$ and $\Delta\varepsilon$ are being varied. For $\Delta\Gamma=0$, keeping $\tilde{\varepsilon}_2=\bar{\varepsilon}_\pm$ fixed and varying only $\tilde{\varepsilon}_1$ (see line "b" in Fig. 2) yields a particularly simple result for the conductance

$$\mathcal{G}_0(\Delta\varepsilon) = \frac{2e^2}{h}\frac{\Gamma^2}{\Delta\varepsilon^2+\Gamma^2}. \tag{11}$$

We see that the line shape in this case is a simple Lorentzian which is, interestingly, independent of t_c. The FWHM reads $\Delta\varepsilon_W=2\Gamma$.

On the other hand, if $t_c<\Lambda=\Gamma$, one can easily show that for fixed $\bar{\varepsilon}=E_F$, the conductance along the $\Delta\varepsilon$ axis reads

$$\mathcal{G}_0(\Delta\varepsilon) = \frac{2e^2}{h}\frac{4\Gamma^2t_c^2}{(\Delta\varepsilon^2+\Gamma^2+t_c^2)^2}, \tag{12}$$

meaning that the line shape is approximately a Lorentzian for $\Delta\varepsilon\ll\sqrt{\Gamma^2+t_c^2}$ and the FWHM is $\Delta\varepsilon_W=2\sqrt{(\sqrt{2}-1)(\Gamma^2+t_c^2)}$. Finally, if we keep $\tilde{\varepsilon}_2$ aligned with E_F and vary only $\tilde{\varepsilon}_1$ (see

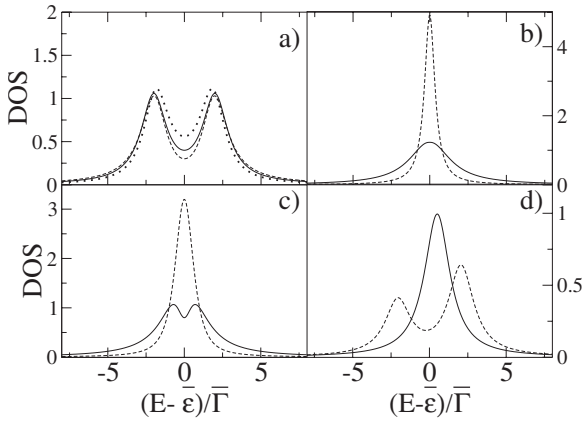

FIG. 5. (a) Local DOS $\rho_1(E)$ for $t_c/\bar{\Gamma}=2$, $\Delta\Gamma=0$ (solid line), and $\rho_1(E)$, $\rho_2(E)$ for $\Delta\Gamma/\bar{\Gamma}=0.6$ (dashed and dotted lines, respectively). (b) Local DOS $\rho_1(E)$, $\rho_2(E)$ (solid and dashed lines, respectively) for $\Delta\Gamma/\bar{\Gamma}=0.6$, $t_c/\bar{\Gamma}=0.1$, and (c) for $t_c/\bar{\Gamma}=0.5$. (d) $\rho_1(E)$ for $\Delta\varepsilon/\bar{\Gamma}=0.5$, $t_c/\bar{\Gamma}=0.1$ (solid line) and $t_c/\bar{\Gamma}=2.0$ (dashed line).

line a in Fig. 3), the conductance as a function of $\Delta\varepsilon$ reads

$$\mathcal{G}_0(\Delta\varepsilon)=\frac{2e^2}{h}\frac{t_c^2}{\Delta\varepsilon^2+\frac{\Gamma^2}{4}\left(1+\frac{t_c^2}{\Gamma^2}\right)^2}. \tag{13}$$

Thus, the line shape is a Lorentzian, which means a weaker $\Delta\varepsilon$ dependence of the conductance than in Eq. (12). This is readily seen in Fig. 3 as high conductance ridges extending further along the $\tilde{\varepsilon}_1$ and $\tilde{\varepsilon}_2$ directions than along the $\Delta\varepsilon$ axis. The width of the resonance is $\Delta\varepsilon_W=(\Gamma^2+t_c^2)/\Gamma$.

To complete our analysis of the zero-temperature physics of our model, we now briefly discuss the local density of states (LDOS) in each of the dots. The LDOS of dot 1 (2) can be obtained from the diagonal matrix elements of the Green's function G_{DD} of the DQD system [see Eq. (A5)]:

$$\rho_i(E)=-\frac{1}{\pi}\Im(G_{DD})_{ii},\quad i=1,2. \tag{14}$$

Our main findings are summarized in Fig. 5. If the levels of the two dots are equal $\tilde{\varepsilon}_1=\tilde{\varepsilon}_2=\bar{\varepsilon}$, then depending on the ratio of the coupling t_c and the asymmetry of the dot-lead couplings $\Delta\Gamma$, one can discern three cases. For $\Delta\Gamma=0$, the LDOS, which is the same in both dots, is a superposition of two Lorentzians centered on energies $E=\bar{\varepsilon}\pm t_c$ [see Fig. 5(a)]. Upon decreasing the ratio $t_c/\Delta\Gamma$, the twin peak structure of the LDOS remains as long as $t_c/\Delta\Gamma>1$ with the LDOS of the dot with smaller dot-lead coupling being larger than that of the other dot's. If the coupling between the dots is weak so that $t_c/\Delta\Gamma\ll 1$ [as in Fig. 5(b)], then the LDOS in each of the dots is basically a Lorentzian of width approximately that of the corresponding couplings $\Gamma_L(\Gamma_R)$. In the intermediate regime of $t_c/\Delta\Gamma\lesssim 1$, an interesting difference in the LDOS of the two dots can be observed [Fig. 5(c)]. The dot having stronger coupling to the corresponding lead has a double peaked LDOS while the other's LDOS is single peaked. If the levels of the dots are detuned ($\Delta\varepsilon\neq 0$), we

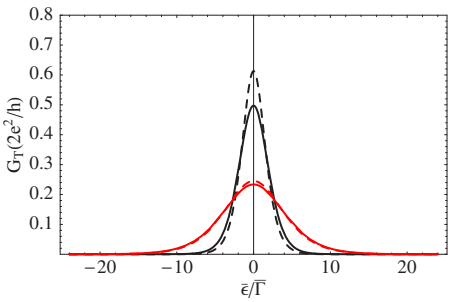

FIG. 6. (Color online) Conductance (in units of $2e^2/h$) as a function of $\bar{\varepsilon}$ for two different temperatures: $k_BT/\bar{\Gamma}=1,2.5$ [black and red (gray) lines, respectively]. Curves with solid lines show the exact result of Eq. (4); the curves with dashed lines are calculated using Eq. (17).

consider the case when $\Delta\Gamma=0$. The LDOS then depends on the ratio $t_c/\Delta\varepsilon$. If the detuning of the levels is large compared to the coupling, i.e., when $t_c/\Delta\varepsilon\ll 1$, the LDOS in dot 1 (2) is peaked at $E=\tilde{\varepsilon}_1$ ($\tilde{\varepsilon}_2$) and has little overlap with the LDOS of the other dot. In the opposite limit of $t_c/\Delta\varepsilon\gg 1$, the LDOS is a superposition of two Lorentzians peaked at the energies of the molecular states $E=\bar{\varepsilon}\pm t_c$.

IV. FINITE-TEMPERATURE LINEAR CONDUCTANCE

We now consider the properties of the conductance for finite temperature. Although the formulas given in Eqs. (4) and (5) are not easily readable, insight into their physical content can again be gained by scanning along certain direction in the $(\tilde{\varepsilon}_1,\tilde{\varepsilon}_2)$ plane, as in the previous section. Let us focus on the case when $|\Delta\Gamma|\neq t_c$, $\Delta\varepsilon\neq 0$ so that the finite-temperature conductance is given by Eq. (4) and let us first address the question of the temperature dependence of conductance in the case of $t_c<\Lambda$, $\Delta\varepsilon=0$. As before, we assume that E_F is kept constant and $\bar{\varepsilon}$ is varied. The energy and temperature dependence of $\mathcal{G}_T$ as given by Eq. (4) is shown by solid lines in Fig. 6. As the temperature increases, the resonance gradually broadens and its height decreases monotonically with T. This behavior can be understood in the limit of $k_BT\gg\Lambda>t_c$ (with $k_BT\ll E_F$). In this case around $\bar{\varepsilon}=E_F$, where the conductance is significant, one finds that $|\omega_\pm|/2\pi=|E_\pm-E_F|/2\pi k_BT\ll 1$ and therefore the expansion of the polygamma functions around 1/2 can be used:

$$\psi^{(1)}\left(\frac{1}{2}+\frac{iz}{2\pi}\right)\approx\frac{\pi^2}{2}+\frac{i\psi^{(2)}(1/2)z}{2\pi}-\frac{\pi^4z^2}{8}+\mathcal{O}(z^3),\quad |\arg z|<\pi. \tag{15}$$

Substituting this expansion into Eq. (4), we find that to leading order in T, the peak height $\mathcal{G}_{T,\max}$ decreases monotonically with the temperature:

$$\mathcal{G}_{T,\max}\approx\frac{2e^2}{h}\frac{\pi}{k_BT}\frac{\Gamma_L\Gamma_R}{\Gamma_L+\Gamma_R}\frac{t_c^2}{(\Gamma_L\Gamma_R+t_c^2)}\quad \text{if } k_BT\gg\Lambda>t_c \text{ and } \Delta\varepsilon=0. \tag{16}$$

A similar $\sim 1/T$ decay can be found for the conductance of a

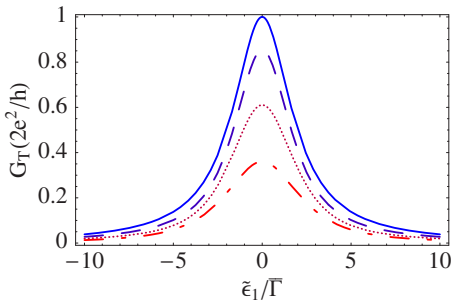

FIG. 7. (Color online) Conductance (in units of $2e^2/h$) as a function of $\tilde{\varepsilon}_1$ for $\tilde{\varepsilon}_2=E_F$ fixed using four different temperatures: $k_BT/\bar{\Gamma}=0,0.5,1.0,2.0$ (solid, dashed, dotted, and dashed-dotted lines, respectively).

single dot.[35] However, the double dot result differs from the result for a single dot by a factor of $2t_c^2/(\Gamma_L\Gamma_R+t_c^2)$, i.e., the degeneracy of the symmetric and antisymmetric levels does not simply contribute a factor of 2 to the conductance as one could naïvely expect but also a factor of $t_c^2/(\Gamma_L\Gamma_R+t_c^2)$. As shown in Fig. 6, for $k_BT\gg\Lambda>t_c$, the conductance is approximated by

$$\mathcal{G}_T(\bar{\varepsilon}) \approx \mathcal{G}_{T,\max}\cosh^{-2}\left(\frac{\bar{\varepsilon}}{2k_BT}\right) \quad \text{if } k_BT\gg\Lambda>t_c \text{ and } \Delta\varepsilon=0, \tag{17}$$

so that apart from the amplitude $\mathcal{G}_{T,\max}$, the line shape is the same as for a single dot. It follows from Eq. (17) that the FWHM is a linear function of the temperature with a slope of 2 $\operatorname{arccosh}(\sqrt{2})$.[8,35] We see that for high temperatures along the $\bar{\varepsilon}$ axes, the conductance of a double dot is similar to that of a single dot with degenerate energy levels.

In contrast to the above behavior, if we keep $\bar{\varepsilon}=E_F$ fixed or $\tilde{\varepsilon}_2=E_F$ fixed and calculate the transmission as a function of $\Delta\varepsilon$ for different temperatures, we see that the resonance peak is not broadened by temperature (Fig. 7). Indeed, if we numerically calculate the FWHM as a function of T using Eq. (4), we see in Fig. 8 (black curve) that in both cases after an initial increase of FWHM in the regime of $k_BT\lesssim\bar{\Gamma}$, the width of the resonance approaches a constant value as the temperature is further increased. For $\Delta\Gamma=0$ using the expansion shown in Eq. (15), we find that for fixed $\bar{\varepsilon}=E_F$, the FWHM is given by

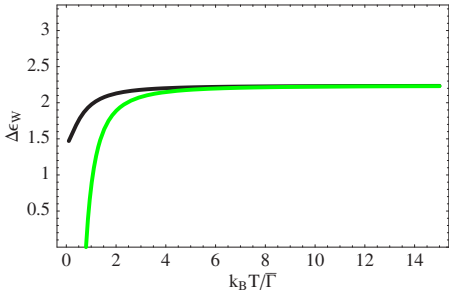

FIG. 8. (Color online) FWHM as a function of temperature along the $\Delta\varepsilon$ axis. The black curve shows the numerically obtained FWHM using Eq. (4); the green (light gray) curve is the function given by Eq. (18). We used $t_c/\Gamma=0.5$.

$$\Delta\varepsilon_{W,T} \approx 2\sqrt{\Gamma^2+t_c^2} - \frac{(\Gamma^2+t_c^2)^{3/2}}{2(k_BT)^2}, \tag{18}$$

therefore, the high-temperature value of the FWHM only weakly increases with temperature since $(\Gamma^2+t_c^2)^{3/2}/(2k_BT)^2 \ll 1$ (see Fig. 8). The ratio of the zero and finite temperature FWHMs is $\Delta\varepsilon_{W,T}/\Delta\varepsilon_W \approx 1.55$ [see $\Delta\varepsilon_W$ after Eq. (12)]. On the other hand, if, e.g., $\tilde{\varepsilon}_2=E_F$ is fixed and $\tilde{\varepsilon}_1$ is changed, a similar calculation yields

$$\Delta\varepsilon_{W,T} \approx 2\sqrt{\Gamma^2+t_c^2} - \frac{(\Gamma^2+t_c^2)^{3/2}}{(k_BT)^2}, \tag{19}$$

thus, $\Delta\varepsilon_{W,T}$ again shows a weak temperature dependence for $k_BT\gtrsim\Gamma$ and compared to the $T=0$ case, we see that $\Delta\varepsilon_{W,T}/\Delta\varepsilon_W \approx 2\Gamma/\sqrt{\Gamma^2+t_c^2}$, which for $\Gamma\gg t_c$ gives $\Delta\varepsilon_{W,T}/\Delta\varepsilon_W \approx 2$. We find therefore that for both scenarios, the FWHM increases as a function of temperature if $k_BT\lesssim\Gamma$ but for $k_BT\gg\Gamma$, it approaches a constant value of $2\sqrt{\Gamma^2+t_c^2}$. This is a remarkable nonthermal broadening effect and is a central result of our paper: while the peak height decreases monotonically with temperature [see Eq. (16)], the width of the peak, when changing only $\Delta\varepsilon$ or $\tilde{\varepsilon}_1$, approaches a constant value, as shown in Eqs. (18) and (19) and in Fig. 8. We emphasize that although for the analytic calculation we assumed $\Delta\Gamma=0$, our numerical results show that the nonthermal broadening is also present for a finite difference in the couplings to the leads, i.e., when $\Delta\Gamma\neq0$. One can also show that for large T, where the FWHM is approximately constant, the line shape of the resonance is approximately a Lorentzian:

$$\mathcal{G}_T(\Delta\varepsilon) = \frac{2e^2}{h}\frac{\pi\Gamma}{k_BT}\frac{t_c^2}{\Delta\varepsilon^2+\Gamma^2+t_c^2} \quad \text{if } k_BT\gg\Gamma>t_c \text{ and } \Delta\Gamma=0. \tag{20}$$

This result holds for both of the scenarios discussed, i.e., either $\bar{\varepsilon}$ or $\tilde{\varepsilon}_2$ being fixed while $\Delta\varepsilon$ is varied.

Let us now consider the case of $t_c>\Lambda$. The temperature dependence of $\mathcal{G}_T$ as given by Eq. (4) along the $\bar{\varepsilon}$ axis is shown in Fig. 9. We see that the conductance peaks gradually broaden and their height decreases with increasing temperature and finally they merge into a single peak for $k_BT\gtrsim t_c$. The maximum of the conductance can then be found at $\bar{\varepsilon}=E_F$ and increasing the temperature further to the regime of $k_BT\gg t_c>\Lambda$, this peak behaves the same way as the case where we assumed $t_c<\Lambda$. This occurs because in the high-temperature limit, k_BT is the largest energy scale in the system and $|\omega_\pm|\ll k_BT$. Hence, the expansion shown in Eq. (15) is applicable and leads to the same results as Eqs. (16)–(19).

For $t_c\gg k_BT,\Lambda$, however, when one can still observe two distinct peaks in the conductance (see, e.g., the green curve in Fig. 9), a different approach has to be employed. Let us focus on the peak at the energy of the symmetric state, i.e., $\bar{\varepsilon}_-=-\sqrt{t_c^2-\Lambda^2}$. (Analogous considerations can be made around the energy $\bar{\varepsilon}_+=\sqrt{t_c^2-\Lambda^2}$ of the antisymmetric state.) If $t_c\gg k_BT,\Lambda$, then for energies around $\bar{\varepsilon}_-$, one finds that

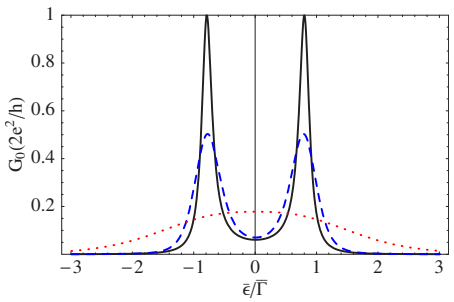

FIG. 9. (Color online) Conductance as a function of $\bar{\varepsilon}$ for three different temperatures: $k_BT/\bar{\Gamma}=0,1,8$ (solid, dashed, and dotted lines, respectively). The ratio of t_c and $\bar{\Gamma}$ is $t_c/\bar{\Gamma}=10$, while $\Delta\Gamma=0$.

$|\omega_+|/2\pi \ll 1$ but $|\omega_-|/2\pi \gg 1$ in Eq. (4). This implies that in the expression of $\mathcal{G}_T$, the polygamma functions, whose argument is ω_-, can be neglected compared with the other two terms, which are functions of ω_+. Indeed, from the expansion of polygamma functions for large arguments

$$\psi^{(1)}(z) \approx \frac{1}{z} + \frac{1}{2z^2} + \frac{1}{6z^3}, \quad z \to \infty, \quad |\arg z| < \pi, \quad (21)$$

it is clear that the contribution of $\psi^{(1)}(1/2 - i\omega_-/2\pi)$ and its complex conjugates in Eq. (4) is very small if $\bar{\varepsilon} \approx \bar{\varepsilon}_-$, which means that for a zero-bias measurement, one can consider the symmetric state as a single resonant level. The finite-temperature conductance around $\bar{\varepsilon}_-$ can then be approximated by

$$\mathcal{G}_T \approx \frac{2e^2}{h} \frac{t_c^2}{\pi(k_BT)^2} \frac{\Gamma_L\Gamma_R}{\Gamma_L+\Gamma_R} \frac{1}{\sqrt{t_c^2-\Delta\Gamma^2}} \times \left[\frac{1}{(\omega_+ - \omega_-^*)} \psi^{(1)}\left(\frac{1}{2} - \frac{i\omega_+}{2\pi}\right) + \text{c.c.} \right] \quad \text{if } t_c \gg k_BT, \Lambda \text{ and } \Delta\varepsilon = 0. \quad (22)$$

In the case k_BT is much larger than Λ, i.e., for $t_c \gg k_BT \gg \Lambda$, one can use the expansion shown in Eq. (15) to obtain further approximations of Eq. (22). For the peak height, we find very similar results to the case of $t_c < \Lambda$. To leading order, the peak height decreases monotonically with temperature:

$$\mathcal{G}_{T,\max} \approx \frac{2e^2}{h} \frac{\pi}{2k_BT} \frac{\Gamma_L\Gamma_R}{\Gamma_L+\Gamma_R} \frac{t_c^2}{(\Gamma_L\Gamma_R + t_c^2)} \quad \text{if } t_c \gg k_BT \gg \Lambda \text{ and } \Delta\varepsilon = 0. \quad (23)$$

Note that there is a factor of 1/2 difference compared to Eq. (16), because the symmetric state behaves as a single resonant level. One also finds that the line shape is rather well approximated by

$$\mathcal{G}_T/\mathcal{G}_{T,\max} \approx \cosh^{-2}\left(\frac{\bar{\varepsilon}-\varepsilon_-}{2k_BT}\right) \quad \text{if } t_c \gg k_BT \gg \Lambda \text{ and } \Delta\varepsilon = 0, \quad (24)$$

especially for $\bar{\varepsilon} \ll \varepsilon_-$. However, due to the other resonant level at energy ε_+, the line shape is, in fact, not symmetric

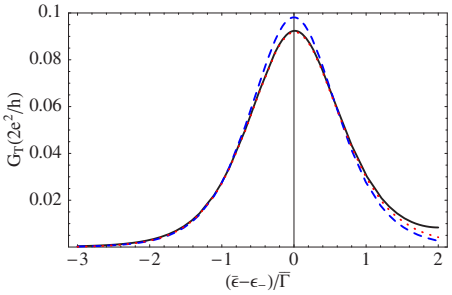

FIG. 10. (Color online) Conductance as a function of $\bar{\varepsilon}$ around the energy of the symmetric state ε_- if $t_c \gg k_BT \gg \bar{\Gamma}$. The exact result of Eq. (4) is shown with solid line, the approximation of Eq. (22) with dotted line, and the formula given by Eq. (24) with dashed line. Parameters: $k_BT/\bar{\Gamma}=8$, $t_c/k_BT=5$, $\Delta\Gamma_L=0$.

around ε_- as Eq. (24) suggests. Comparison of the exact result given by Eq. (4) with the approximations of Eqs. (22) and (24) is shown in Fig. 10. A small but noticeable deviation of the approximation given by Eq. (24) from the exact result Eq. (4) can indeed be observed for $\bar{\varepsilon} \gtrsim \varepsilon_-$, while Eq. (22) gives a better approximation over the whole energy range around ε_-.

For the properties of the conductance along the $\Delta\varepsilon$ axes or along the $\tilde{\varepsilon}_1$ axes, the characteristic energies $\Delta\varepsilon_{W,T}$ for each case can be calculated using Eq. (22) and the expansion shown in Eq. (15). The resulting formulas are, however, rather complicated and not too informative. Numerical calculations shown in Fig. 11 clearly indicate that the resonance is broadened by temperature in the regime of $t_c \gg k_BT, \Gamma$.

We can conclude therefore that in the studied system, the nonthermal broadening of the conductance resonance occurs only if k_BT is the largest energy scale.

V. CONCLUSIONS

In conclusion, we have studied the linear conductance of a double quantum dot molecule at zero and finite temperatures. We have found that the coupling of the dots to the leads produces level attraction, which depends both on the total coupling strength $\bar{\Gamma}$ and on the asymmetry $\Delta\Gamma$ of the couplings. We have discussed the properties of the conductance

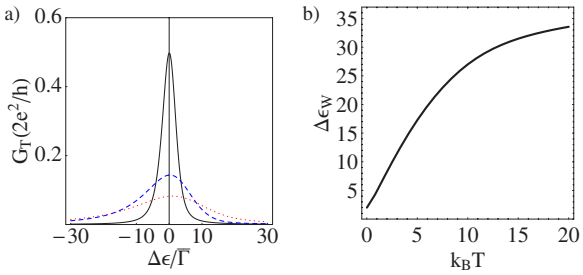

FIG. 11. (Color online) The conductance as a function of $\Delta\varepsilon$ for three different temperatures: $k_BT/\Gamma=1,5,10$ (solid, dashed, and dotted lines, respectively) and fixed $\tilde{\varepsilon}_1=\varepsilon_-$ (a). The numerically calculated FWHM using Eq. (4) as a function of temperature (b). We used $\Delta\Gamma=0$ and $t_c/\Gamma=20$.

when the interdot coupling t_c is larger (smaller) than this level attraction. In particular, at zero temperature, we have given explicit expression for the line shape of the conductance in the $(\tilde{\varepsilon}_1, \tilde{\varepsilon}_2)$ plane along certain experimentally important axes. Considering the finite-temperature conductance, we have discussed the temperature dependence and the line shape of the conductance along these axes. We have shown that if the temperature is the largest energy scale in the system, the conductance resonance, which arises due to the detuning of the energy levels of the quantum dots, is not broadened by the temperature. Our results can be relevant for understanding of those recent experimental results where an effective single-particle description is adequate.

ACKNOWLEDGMENTS

Enlightening discussions with András Csordás are gratefully acknowledged. This work is supported by EC Contract No. MRTN-CT-2003-504574 and EPSRC.

APPENDIX A

In this appendix, we derive the electron transmission coefficient through serially coupled, coherent quantum dots, connected to multichannel leads. There are numerous equivalent approaches in computing transport through such phase-coherent structures, including recursion methods and transfer matrix techniques.[42,43] Here, we employ the Green's-function method and notation presented in Ref. 44, in which the Hilbert space is divided into a subspace A containing the external leads and a subspace B containing the two dots.

We start by considering isolated left and right dots, which are each described by a single quantum state $|f_1\rangle$ and $|f_2\rangle$, with energy levels ε_1 and ε_2, respectively. When these are coupled together by a Hamiltonian h_{12}, the 2×2 Green's function g_B of the coupled dots is given by

$$g_D^{-1} = \begin{pmatrix} g_{11}^{-1} & -t_c \\ -t_c^* & g_{22}^{-1} \end{pmatrix}, \tag{A1}$$

where $t_c = \langle f_1|h_{12}|f_2\rangle$ and $g_{jj}^{-1} = E - \varepsilon_j$. [This representation is convenient because the self-energy matrix in Eq. (A5) below is then diagonal.]

The effect of coupling the left (right) dot to the left (right) lead via a coupling matrix W_1 (W_2) is represented by self-energies $\Sigma_L = \sigma_L - i\Gamma_L$ ($\Sigma_R = \sigma_R - i\Gamma_R$) (where $\sigma_L, \Gamma_L, \sigma_R, \Gamma_R$ are real) defined by

$$\Sigma_L = \sum_{n_L} \langle f_1|W_1^\dagger|n_L\rangle g_A(n_L)\langle n_L|W_1|f_1\rangle, \tag{A2}$$

and

$$\Sigma_R = \sum_{n_R} \langle f_2|W_2^\dagger|n_R\rangle g_A(n_R)\langle n_R|W_2|f_2\rangle, \tag{A3}$$

where $|n_{L(R)}\rangle$ is a channel state belonging to the L (R) lead and $g_A(n_{L(R)})$ is the channel Green's function, such that

$$g_A^{L(R)} = \sum_{n_L(n_R)} |n_{L(R)}\rangle g_A(n_{L(R)})\langle n_{L(R)}| \tag{A4}$$

is the corresponding surface Green's function.

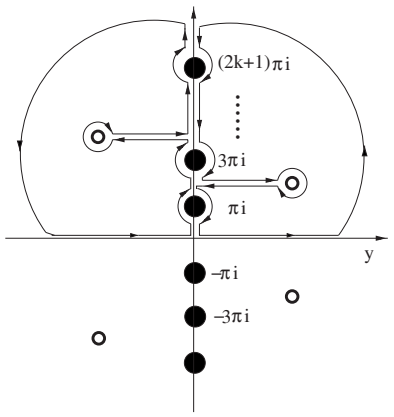

FIG. 12. The two integration contours to calculate the integral in Eq. (3). Filled circles denote the second order poles of $-\frac{\partial f_0(E)}{\partial E}$; open circles show the poles of $T_{dd}(E)$.

In the presence of the leads, the Green's function G_{BB} of the double dot is given by

$$G_{DD}^{-1} = g_D^{-1} - \begin{pmatrix} \Sigma_L & 0 \\ 0 & \Sigma_R \end{pmatrix}, \tag{A5}$$

which yields the transmission coefficient T_{dd} via the formula

$$T_{dd} = 4\,\mathrm{Tr}[\Gamma(L)G_{DD}\Gamma(R)G_{DD}^\dagger] = 4\Gamma_L\Gamma_R|(G_{DD})_{12}|^2, \tag{A6}$$

where

$$\Gamma(L) = \begin{pmatrix} \Gamma_L & 0 \\ 0 & 0 \end{pmatrix}, \tag{A7}$$

and

$$\Gamma(R) = \begin{pmatrix} 0 & 0 \\ 0 & \Gamma_R \end{pmatrix}. \tag{A8}$$

Finally, from Eq. (A5),

$$(G_{DD})_{12} = t_c/[(E - \varepsilon_1 - \sigma_L + i\Gamma_L)(E - \varepsilon_2 - \sigma_R + i\Gamma_R) - |t_c|^2], \tag{A9}$$

and writing $\tilde{\varepsilon}_1 = \varepsilon_1 + \sigma_L$ and $\tilde{\varepsilon}_2 = \varepsilon_2 + \sigma_R$ yields Eq. (1) of the main text.

We note that this equation resembles Eq. (20) of Ref. 41. However, the latter omits the self-energy terms σ_L and σ_R, which in general are non-negligible.

APPENDIX B

Introducing the dimensionless variable $y = (E - E_F)/k_BT$, the integral I in Eq. (3) reads

$$I = \frac{4\Gamma_L\Gamma_R t_c^2}{(k_BT)^4}\int_{-\infty}^{\infty} \frac{dy f'(y)}{(y - \bar{\omega}_+)(y - \bar{\omega}_+^*)(y - \bar{\omega}_-)(y - \bar{\omega}_-^*)}, \tag{B1}$$

where $f'(y) = 1/\cosh^2\left(\frac{y}{2}\right)$ and $\bar{\omega}_\pm = (E_\pm - E_F)/k_BT$. This integral can be calculated using contour integration. Care has to

be taken, however, because the integrand is not bounded on the imaginary axes. Nevertheless, one can calculate this integral as a sum of two contour integrals, as shown in Fig. 12.

Closing the contours in the upper half plane, the contributions of the two contours along the imaginary axes cancel, except around the (second order) poles of the derivative of the Fermi function $f_0(E)$ (shown by filled circles in Fig. 12). These poles are located at $(2k+1)i\pi$, where k is an integer. The other contribution to the integral comes from the poles $E_\pm$ of the transmission function $T_{dd}(E)$ (denoted by open circles in Fig. 12). Summing all the contributions from the poles and using the series expansions of the first polygamma function[31]

$$\psi^{(1)}(z) = \sum_{k=0}^{\infty} \frac{1}{(z+k)^2}, \tag{B2}$$

and of the $1/\cos^2(z)$ function

$$\frac{1}{\cos^2(z)} = 4\sum_{k=0}^{\infty} \left\{ \frac{1}{[(2k+1)\pi - z]^2} + \frac{1}{[(2k+1)\pi + z]^2} \right\}, \tag{B3}$$

one can finally obtain the result shown in Eq. (4).

[1] Y. V. Nazarov, Physica B **189**, 57 (1993).
[2] G. Klimeck, G. Chen, and S. Datta, Phys. Rev. B **50**, 2316 (1994).
[3] N. C. van der Vaart, S. F. Godijn, Y. V. Nazarov, C. J. P. M. Harmans, J. E. Mooij, L. W. Molenkamp, and C. T. Foxon, Phys. Rev. Lett. **74**, 4702 (1995).
[4] F. R. Waugh, M. J. Berry, D. J. Mar, R. M. Westervelt, K. L. Campman, and A. C. Gossard, Phys. Rev. Lett. **75**, 705 (1995).
[5] F. R. Waugh, M. J. Berry, C. H. Crouch, C. Livermore, D. J. Mar, R. M. Westervelt, K. L. Campman, and A. C. Gossard, Phys. Rev. B **53**, 1413 (1996).
[6] Cheng Niu, Li-jun Liu, and Tsung-han Lin, Phys. Rev. B **51**, 5130 (1995).
[7] K. A. Matveev, L. I. Glazman, and H. U. Baranger, Phys. Rev. B **54**, 5637 (1996).
[8] R. Kotlyar and S. Das Sarma, Phys. Rev. B **56**, 13235 (1997).
[9] C. A. Stafford, R. Kotlyar, and S. Das Sarma, Phys. Rev. B **58**, 7091 (1998).
[10] T. Pohjola, J. König, H. Schoeller, and G. Schön, Phys. Rev. B **59**, 7579 (1999).
[11] R. Ziegler, C. Bruder, and H. Schoeller, Phys. Rev. B **62**, 1961 (2000).
[12] R. H. Blick, R. J. Haug, J. Weis, D. Pfannkuche, K. v. Klitzing, and K. Eberl, Phys. Rev. B **53**, 7899 (1996).
[13] R. H. Blick, D. Pfannkuche, R. J. Haug, K. v. Klitzing, and K. Eberl, Phys. Rev. Lett. **80**, 4032 (1998).
[14] M. Pi, A. Emperador, M. Barranco, F. Garcias, K. Muraki, S. Tarucha, and D. G. Austing, Phys. Rev. Lett. **87**, 066801 (2001).
[15] M. Pioro-Ladrière, M. Ciorga, J. Lapointe, P. Zawadzki, M. Korkusiński, P. Hawrylak, and A. S. Sachrajda, Phys. Rev. Lett. **91**, 026803 (2003).
[16] W. G. van der Wiel, S. De Franceschi, J. M. Elzerman, T. Fujisawa, S. Tarucha, and L. P. Kouwenhoven, Rev. Mod. Phys. **75**, 1 (2003).
[17] T. Ota *et al.*, Phys. Rev. Lett. **93**, 066801 (2004).
[18] A. K. Hüttel, S. Ludwig, H. Lorenz, K. Eberl, and J. P. Kotthaus, Phys. Rev. B **72**, 081310(R) (2005).
[19] T. Hatano, M. Stopa, and S. Tarucha, Science **309**, 268 (2005).
[20] M. R. Gräber, W. A. Coish, C. Hoffmann, M. Weiss, J. Furer, S. Oberholzer, D. Loss, and C. Schönenberger, Phys. Rev. B **74**, 075427 (2006).
[21] S. Sapmaz, C. Meyer, P. Beliczynski, P. Jarillo-Herrero, and L. P. Kouwenhoven, Nano Lett. **6**, 1350 (2006).
[22] M. J. Biercuk, S. Garaj, N. Mason, J. M. Chow, and C. M. Marcus, Nano Lett. **5**, 1267 (2005).
[23] H. I. Jørgensen, K. Grove-Rasmussen, J. R. Hauptmann, and P. E. Lindelof, Appl. Phys. Lett. **89**, 232113 (2006).
[24] C. Fasth, A. Fuhrer, M. T. Björk, and L. Samuelson, Nano Lett. **5**, 1487 (2005).
[25] A. Pfund, I. Shorubalko, R. Leturcq, and K. Ensslin, Appl. Phys. Lett. **89**, 252106 (2006).
[26] H. Jeong, A. M. Chang, and M. R. Melloch, Science **293**, 2221 (2001).
[27] J. C. Chen, A. M. Chang, and M. R. Melloch, Phys. Rev. Lett. **92**, 176801 (2004).
[28] A. W. Rushforth, C. G. Smith, I. Farrer, D. A. Ritchie, G. A. C. Jones, D. Anderson, and M. Pepper, Phys. Rev. B **73**, 081305(R) (2006).
[29] D. M. Schröer, A. K. Hüttel, K. Eberl, S. Ludwig, M. N. Kiselev, and B. L. Altshuler, Phys. Rev. B **74**, 233301 (2006).
[30] D. Loss and D. P. DiVincenzo, Phys. Rev. A **57**, 120 (1998).
[31] M. Abramowitz and I. A. Stegun, *Handbook of Mathematical Functions* (Dover, New York, 1972).
[32] Supriyo Datta, *Electronic Transport in Mesoscopic Systems* (Cambridge University Press, Cambridge, 1995).
[33] M. L. Ladrón de Guevara, F. Claro, and P. A. Orellana, Phys. Rev. B **67**, 195335 (2003).
[34] B. Kubala and J. König, Phys. Rev. B **65**, 245301 (2002).
[35] C. W. J. Beenakker, Phys. Rev. B **44**, 1646 (1991).
[36] R. Aguado and D. C. Langreth, Phys. Rev. Lett. **85**, 1946 (2000).
[37] T. Aono and M. Eto, Phys. Rev. B **63**, 125327 (2001).
[38] R. López, Ramón Aguado, and Gloria Platero, Phys. Rev. Lett. **89**, 136802 (2002).
[39] P. A. Orellana, G. A. Lara, and E. V. Anda, Phys. Rev. B **65**, 155317 (2002).
[40] B. R. Bułka and T. Kostyrko, Phys. Rev. B **70**, 205333 (2004).
[41] A. I. Larkin and K. A. Matveev, Zh. Eksp. Teor. Fiz. **93**, 1030 (1987) [Sov. Phys. JETP **66**, 580 (1987)].
[42] C. J. Lambert, J. Phys. C **17**, 2401 (1984).
[43] C. J. Lambert, Phys. Rev. B **29**, 1091 (1984).
[44] N. R. Claughton, M. Leadbeater, and C. J. Lambert, J. Phys.: Condens. Matter **7**, 8757 (1995).